

Fourier pulse-shaper-based high-order differential group delay emulator

S. X. Wang and A. M. Weiner

School of Electrical & Computer Engineering, Purdue University, West Lafayette, IN 47907-1285, USA
wang7@ecn.purdue.edu, amw@ecn.purdue.edu

Abstract: We demonstrate a Fourier pulse-shaper-based differential group delay (DGD) emulator which can be programmed to possess arbitrary user-specified frequency dependent DGD profile. The DGD produced can be up to 400ps range with <1ps accuracy. Generated frequency-dependent DGD profiles are in excellent agreement with numerical simulations.

©2007 Optical Society of America

OCIS codes: (260.5430) Polarization; (060.2330) Fiber optics communications; (060.2270) Fiber characterization; (320.5540) Pulse shaping.

References and links

1. G. J. Foschini and C. D. Poole, "Statistical theory of polarization dispersion in single mode fibers," *J. Lightwave Technol.* **9**, 1439-1456 (1991).
2. I. Kaminow, "Polarization mode dispersion" in *Optical Fiber Communications IVb*, Ed. (San Diego, CA, Academic Press, 745-762 (2002).
3. G. Biondini, W. L. Kath, and C. R. Menyuk, "Importance Sampling for PMD," *IEEE Photon. Technol. Lett.* **14**, 310-312 (2002).
4. L. Yan, M. C. Hauer, Y. Shi, X. S. Yao, P. Ebrahimi, Y. Wang, A. E. Willner, and W. L. Kath, "PMD Emulator using variable DGD elements and its use for experimental importance sampling," *J. Lightwave Technol.* **22**, 1051-1058 (2004).
5. I. T. Lima, R. Khosravani, P. Ebrahimi, E. Ibragimov, C. R. Menyuk, and A. E. Willner, "Comparison of polarization mode dispersion emulators," *J. Lightwave Technol.* **19**, 1872-1881 (2001).
6. R. Chipman and R. Kinnera, "High-order polarization mode dispersion emulator," *Opt. Eng.* **41**, 932-937 (2002).
7. D. S. Waddy, et al., "High-order PMD and PDL emulation," *Optical Fiber Communication Conference, ThF6*, Los Angeles, CA, (2004).
8. M. Wegmuller, S. Demma, C. Vinegoni, and N. Gisin, "Emulator of first- and second-order polarization-mode dispersion," *IEEE Photon. Technol. Lett.* **14**, 630-632 (2002).
9. M. Akbulut, R. Nelson, A. M. Weiner, P. Cronin, and P. J. Miller, "Broadband polarization correction with programmable liquid-crystal modulator arrays," *Opt. Lett.* **29**, 1129-1131 (2004).
10. P. B. Phua, H. A. Haus, and E. P. Ippen, "All-frequency PMD compensator in feedforward scheme," *J. Lightwave Technol.* **22**, 1280-1288 (2004).
11. A. M. Weiner, "Femtosecond pulse shaping using spatial light modulators," *Rev. Sci. Instrum.* **71**, 1929-1960 (2000).
12. R. D. Nelson, D. E. Leaird, and A. M. Weiner, "Programmable polarization-independent spectral phase compensation and pulse shaping," *Opt. Express.* **11**, 1763-1769 (2003).
13. G. H. Lee, S. Xiao, A. M. Weiner, "Optical dispersion compensator with >4000-ps/nm tuning range using a Virtually Imaged Phased Array (VIPA) and Spatial Light Modulator (SLM)," *IEEE Photon. Technol. Lett.* **18**, 1819-1821 (2006).
14. M. Shirasaki, "Large Angular Dispersion by a Virtually Imaged Phased Array and its application to a wavelength demultiplexer," *Opt. Lett.* **21**, 366-368 (1996).
15. S. Xiao, A. M. Weiner, and C. Lin, "A dispersion law for virtually imaged phased-array spectral dispersers based on paraxial wave theory," *IEEE J. Quantum Electron.* **40**, 420-426 (2004).
16. T. Brixner, G. Gerber, "Femtosecond polarization pulse shaping," *Opt. Lett.* **26**, 557-559 (2001).
17. S. X. Wang, A. M. Weiner, "Fast wavelength-parallel polarimeter for broadband optical networks," *Opt. Lett.* **29**, 923-925 (2004).
18. L. Polachek, D. Oron, Y. Silberberg, "Full control of the spectral polarization of ultrashort pulses," *Opt. Lett.* **31**, 631-633 (2006).
19. M. Akbulut, A. M. Weiner, and P. J. Miller, "Wideband all-order polarization mode dispersion compensation via pulse shaping," *Opt. Lett.* **30**, 2691-2693 (2005).

1. Introduction

The instantaneous polarization mode dispersion (PMD) of an optical fiber can be characterized by a frequency dependent PMD vector $\mathbf{\Omega}(\omega)$, with its direction defining the fiber's principal states of polarization (PSP) and its magnitude defining the differential group delay (DGD). Due to the statistical nature of PMD, a PMD emulator is an important tool for characterizing PMD effects in an optical fiber system by cycling through the various PMD states expected in an optical fiber. Since DGD follows a Maxwellian distribution [1] and system outages are most likely to happen in the low probability tail of the distribution curve, it is inefficient for the PMD emulators to run at random and wait for the occasional outages. System designers typically require that system outage due to PMD occur with a probability of 10^{-6} or less (<1min/year) [2]. To efficiently study PMD, importance sampling is commonly used for obtaining low probability events with relatively fewer sample points [3]. Such low probability events typically involve instances of large DGD, for which higher-order (frequency dependent) PMD terms become increasingly pronounced [2]. Therefore, to incorporate importance sampling techniques experimentally using a PMD emulator, user-specified control of the frequency-dependent PMD profile is desired for obtaining the rare PMD events [4].

The simplest type of PMD emulator is of the first order, which incorporates a pair of polarizing beam splitters in a split-and-recombine configuration. One of the optical paths contains a variable optical delay line, thus controlling the DGD between the two paths. Although the amount of DGD of a first-order PMD emulator can be deterministically controlled, by definition the DGD produced cannot be varied over frequency. Current high-order PMD emulators are based on the concept of a series of birefringent elements with independently tunable DGD or coupling angles [4]-[8] to mimic the randomness of PMD in a real fiber. While statistical tunability of the produced DGD has been reported using this type of emulator design [4], generation of specific frequency-dependent DGD profiles desired by the user may be difficult. In the next section, we describe a new method for emulation which enables generation of essential arbitrary user-defined frequency-dependent DGD profiles. The emulator contains no mechanical components which makes it repeatable. First-order PMD range has been tested up to 400ps with an accuracy of within ± 1 ps. Frequency dependent DGD profiles have also been programmed onto the emulator and demonstrate excellent agreement with simulated results. This arbitrary controllability is an important feature which allows user specified DGD statistics to be produced, and will allow IS technique to be implemented more easily. It will also open up new possibilities for testing PMD in systems, such as independently studying effects due to various orders of PMD.

Note that in our current apparatus, the directions of the principal states of polarization remain constant for all frequencies. However, a wavelength-parallel polarization controller demonstrated in our laboratory [9] can be used in tandem with the current DGD emulator to control the PSP directions and hence realize an all-order PMD emulator. Although in this paper we are describing a DGD emulator, however one can envision that this device could also be used in reverse as an all-order DGD compensator. Provided that the DGD is known and fed-back into the DGD compensator, our apparatus could be used in realizing a full, high-order PMD compensator of the type proposed by Phua et. al., [10].

2. DGD emulator theory

The Jones Matrix of a birefringent medium can be written as:

$$T(\omega) = e^{-j\psi(\omega)} \begin{bmatrix} e^{j\phi(\omega)} & 0 \\ 0 & e^{-j\phi(\omega)} \end{bmatrix}, \quad (1)$$

where $\psi(\omega)$ is the common-mode phase and $2\phi(\omega)$ is the phase difference introduced by the two axes of the medium. Since we are only interested in the differential phase, we set $\psi(\omega)=0$. By controlling the spectral phase $\phi(\omega)$, and programming the two principal axes of the birefringent medium for equal and opposite spectral phase, one can control the group delays $\tau^+(\omega)$ and $\tau^-(\omega)$ of the slow and fast PSP axes through the relation

$$\tau^-(\omega) = -\tau^+(\omega) = \frac{d\phi(\omega)}{d\omega} \quad (2)$$

The DGD is the group delay difference between the slow and the fast PSP axes and can be controlled through the relation

$$\Delta\tau(\omega) = \tau^+(\omega) - \tau^-(\omega) = \frac{-2d\phi(\omega)}{d\omega} \quad (3)$$

While adjusting the phase to have desired nonlinear frequency variation, one can generate higher order DGD profiles, defined in a Taylor series about the center frequency ω_0 as

$$\Delta\tau(\omega) = 2\tau + 2\tau_{\omega}(\omega - \omega_0) + \tau_{\omega\omega}(\omega - \omega_0)^2 + \dots \quad (4)$$

Here, τ , τ_{ω} , $\tau_{\omega\omega}$ are used as coefficients to the polynomial and are respectively the shorthand representations of $\tau(\omega_0)$, $\left. \frac{d\tau(\omega)}{d\omega} \right|_{\omega_0}$, and $\left. \frac{d^2\tau(\omega)}{d\omega^2} \right|_{\omega_0}$. 2τ is the 1st order PMD (constant DGD),

the second term gives a DGD profile varying linearly with frequency, and the third term gives a quadratic frequency-dependent DGD profile. Next, we describe a DGD emulator which operates via control of the spectral phase, and can be programmed to generate essentially any user-defined frequency-dependent $\Delta\tau(\omega)$ profile.

3. Experimental setup

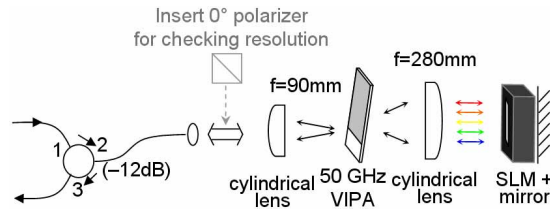


Fig. 1. VIPA pulse shaper based DGD emulator.

In a Fourier pulse shaper [11, 12, 13], the time domain pulse can be arbitrarily shaped by controlling the phase and amplitude of its Fourier counterpart in the spectral domain. Our DGD emulator design is based on a Fourier pulse shaper in the sense that the spectral phase of the incident light pulse is controlled in a wavelength-parallel scheme. The difference is that the phases on two orthogonal polarization axes are controlled independently to introduce a differential phase as needed by Eqs. (2) and (3) to obtain DGD. In particular, the phases applied to the two orthogonal axes are chosen to be equal but opposite. Conversely, the reader may notice that when the phases on the two orthogonal polarization axis are programmed in common mode, the setup becomes a polarization-independent phase pulse shaper, which enables generation of programmable, isotropic, frequency-dependent chromatic dispersion [12]. The three main components of the emulator include a circulator, a Virtually Imaged Phased Array (VIPA) spectral disperser [14, 15] with 50 GHz free spectral range

(FSR), and a dual-layer, 128-element nematic liquid crystal spatial light modulator (SLM) as shown in Fig. 1. The input light was spectrally dispersed using the VIPA onto the SLM, which ran in a double-pass (reflective) scheme with a mirror. The VIPA device is polarization independent and does not require compensation of polarization-dependent loss as in typical grating-based polarization pulse shapers [16]. The optic axes of the two layers of the SLM were respectively 45° and 135° , with each layer controlling the phase profile of the field polarized along its designated direction as described in Eq. (1). By using two layers with orthogonal optic axes (i.e. 45° and 135°), the two orthogonal principal states can be defined, and DGD between the two principal states could be controlled. The group delay of each principal state of polarization comes from the frequency variation of phase introduced by the SLM. The desired phase profile is programmed onto the SLM modulo 2π , so a maximum phase swing of only 2π per pixel is required. The update speed of the SLM is on the order of tens of ms, limited by the liquid crystal relaxation time. Since there are multiple diffraction orders and only the main one is used (other diffraction orders from the VIPA are physically blocked), the insertion loss of the system was measured at $\geq 12\text{dB}$.

To check the resolution of the DGD emulator, a 0° polarizer was inserted at the output of the collimator to allow the pulse shaper to perform amplitude modulation (see Fig. 1). Then a tunable laser was used for obtaining the amplitude transfer function of the pulse shaper via swept-wavelength measurement with 1pm sweep resolution. With only pixel #63 (center of the SLM) programmed for total transmission, the measured 3dB spectral resolution was $\sim 0.74\text{GHz}$. Pixel #64 alone was then programmed for transmission, and the frequency peaks from the two individual measurements of pixel #63 and #64 were compared to give a SLM pixel spacing of $\sim 0.76\text{GHz}$. Realizing that phase control is pixelated from the SLM, finite approximation will be used for Eq. (3):

$$\Delta\tau(\omega) = \tau^+(\omega) - \tau^-(\omega) = -2 \frac{\Delta\phi(\omega)}{\Delta\omega} \quad (5)$$

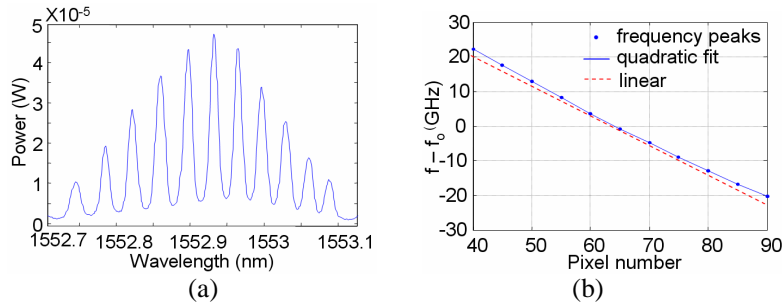


Fig. 2. (a). One out of every 5 SLM pixels turned on to check wavelength-to-pixel mapping. (b) Quadratic fit to the frequencies corresponding to the wavelength peaks in (a), which yields the pixel vs. frequency mapping.

Due to the frequency dependence of the spectral dispersion of the VIPA [15], the pixel-to-pixel frequency spacing $\Delta\omega$ is not constant throughout the pixel array. Therefore directly programming a constant $\Delta\phi(\omega)$ between neighboring pixels (linear phase vs. pixel number example) will yield an unwanted quadratic spectral phase. Therefore the precise frequency mapped onto each pixel must be found in order to correctly program the desired phase profile. To perform this task, a broadband amplified spontaneous emission (ASE) source was input into the emulator, and every fifth pixel was programmed for transmission. The wavelength at each peak was found using an optical spectrum analyzer and the corresponding frequencies were plotted against the transmissive pixels as shown in Fig. 2. As can be seen, the curve deviated from the desired linear line. A quadratic fit

$$\omega(n) = a(n - n_0)^2 + b(n - n_0) + \omega_0 \quad (6)$$

was applied to the resultant curve in angular frequency and the coefficients a and b were found to be 1.73×10^7 rad/s/pixel² and -7.6×10^9 rad/s/pixel respectively. Here ω_0 is the center frequency at a pixel designated as n_0 . By integrating Eq. (4), and substituting $n-n_0$ for ω , the differential phase equation between the two layers of the SLM can be obtained:

$$2\phi(n) = -2\tau(a(n-n_0)^2 + b(n-n_0)) - \tau_{\omega}(a(n-n_0)^2 + b(n-n_0))^2 - \frac{1}{3}\tau_{\omega\omega}(a(n-n_0)^2 + b(n-n_0))^3 + \dots \quad (7)$$

The slow axis is defined by the SLM layer with $-\phi(n)$ and the fast axis with $\phi(n)$.

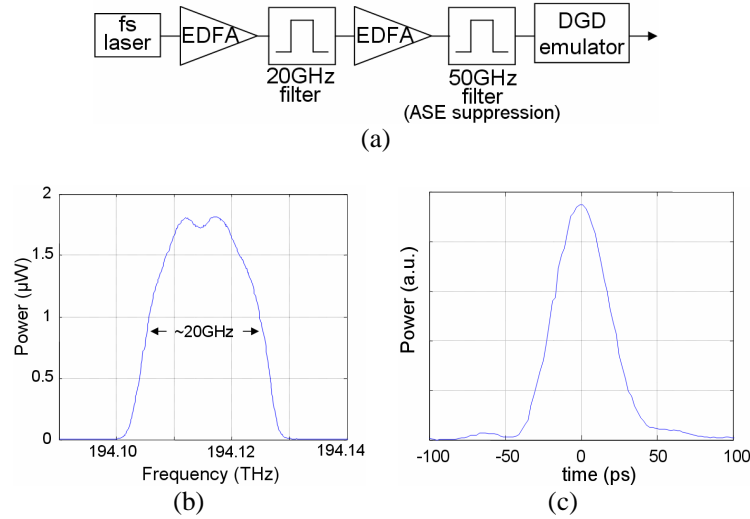


Fig. 3. (a). Experimental setup (b) Output power spectrum (c) Output time domain pulse with DGD=0.

The source used for testing the emulator was a mode-locked laser [see Fig. 3(a)], amplified using an erbium doped fiber amplifier (EDFA) and filtered to reduce the bandwidth down to 20GHz. The 20GHz filter was constructed using a diffraction grating based Fourier pulse shaper with its SLM replaced by a slit. The slit allows the selection of a 20GHz frequency range with very steep roll off, which is very important for keeping the power within one free spectral range of the VIPA; otherwise there will be oscillations in the time domain caused by the beating between frequency components transmitted by different VIPA passbands that repeat with period equal to the FSR. A second EDFA was used to compensate the loss of this filtering process. Finally, a 50GHz filter was added to suppress the ASE noise of the second EDFA. The resulting spectral profile with ~20GHz full width at half maximum is shown in Fig. 3(b). The resultant time domain pulse after filtering was roughly 50ps is shown in Fig. 3(c), which was measured using a 50GHz photodiode and a fast sampling scope. The 50ps pulse width indicates that the pulse was bandwidth limited. This 50ps pulse resembled a digital bit in a 10Gb/s return-to-zero system. The periodic-in-frequency character of a pulse shaper constructed using a VIPA spectral disperser constrains the application of the emulator to signals whose modulation bandwidths are less than one FSR of the VIPA. To accommodate larger signal bandwidths, a VIPA with larger free spectral range should be used.

4. Experimental results

In this section we measure the effects of various DGD profiles programmed onto the pulse. Different DGD profiles were programmed onto the DGD emulator by setting different values to the coefficients described in Eq. (4). The resulting time domain profiles were measured by the same photodiode and fast sampling scope setup with approximately equal power launched into each PSP. First, we test constant DGD by setting only τ nonzero for Eq. (4). Figure 4 shows a time domain measurements of some sample emulations of constant DGDs. For small DGD values of less than 50ps, the pulse split is not obvious, therefore two different traces were taken: one trace when the pulse is polarization controlled to the fast axis, and the other when it is controlled to the slow axis. To reduce noise in the measurements, the pulses are first fit using high order (40th) polynomial [shown in red in Figs. 4(a)-4(d)], and the DGD is calculated as the difference between the two pulse peaks. The amount of programmed DGD was tested from 0ps to 400ps with observed accuracy of within ± 1 ps. The range of DGD that can be generated is limited by the temporal windowing effect resulting from the finite spectral resolution due to the SLM pixelation and the finite spot size at the SLM plane [11]. The temporal windowing envelopes the peaks of each pair of pulses with various amounts of $\Delta\tau$, as can be seen in Fig. 4(e). System designers typically require mean DGD to be less than 15% of the bit duration, e.g. 15ps in a 10Gb/s system, and PMD stress tests will not likely surpass a DGD value of 100ps. Therefore, the temporal windowing effect is small within the ± 100 ps DGD range of greatest interest for this emulator.

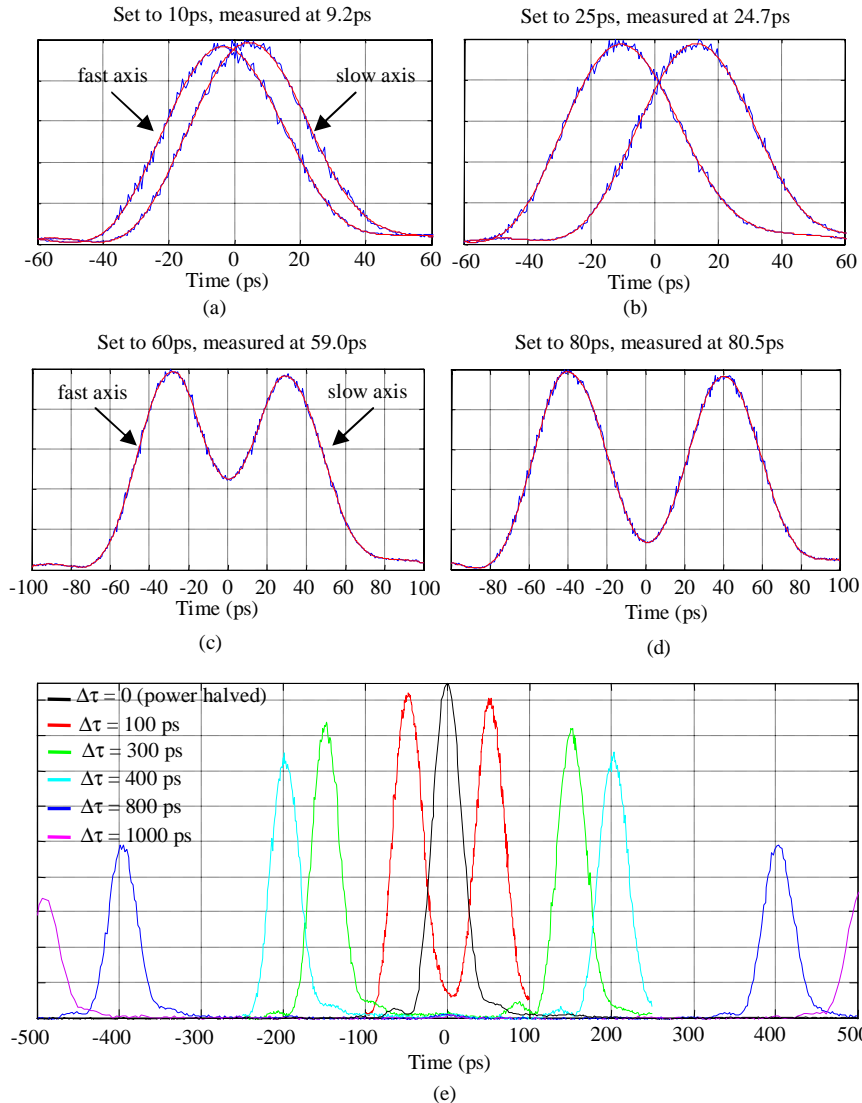


Fig. 4. Time domain pulse splitting due to constant DGD with 2τ equal to (a) 10ps, (b) 25ps, (c) 60ps, (d) 80ps. (e) Temporal windowing effect shown by large DGD values, power halved at $\Delta\tau=0$ to account of the merging of the pair of pulses.

We also performed experiments in which frequency-dependent DGD profiles were applied. For comparison, theoretical results were obtained by taking the Fourier transform of the measured optical spectrum with the applied values of $\phi(\omega)$ added. Figure 5 shows the resultant pulse with 400ps constant DGD plus various amounts of DGD linear in frequency. The linear DGD component represents polarization dependent chromatic dispersion. The original pulse splits into two pulses separated by 400ps, with each of the pulses broadened due to the (opposite) chromatic dispersion on their respective PSP axes. It is worth noticing that the shape of each pulse in Fig. 5(d) resembles the shape of the spectrum shown in Fig. 3(c); this is expected behavior which results when large enough chromatic dispersion causes optical frequency components to separate linearly in time, tracing the shape of the spectral power density in time. Finally, we programmed the emulator with various quadratic DGD

along with 600ps of constant DGD. The resultant pulses split by 600ps, and each carried a “tail” due to 3rd order phase as can be seen in Fig. 6. The slight difference in height between the left and the right pulses was caused by uneven power splitting between the two PSP, and was taken into account in the simulation as well. As shown from the figures, the programmed emulator with various amount of DGD matched the theoretical DGD profiles very well. Although only up to 3rd order phase difference (quadratic DGD) was tested, the programmability of our system signifies that virtually any arbitrary DGD vs. frequency profile can be emulated.

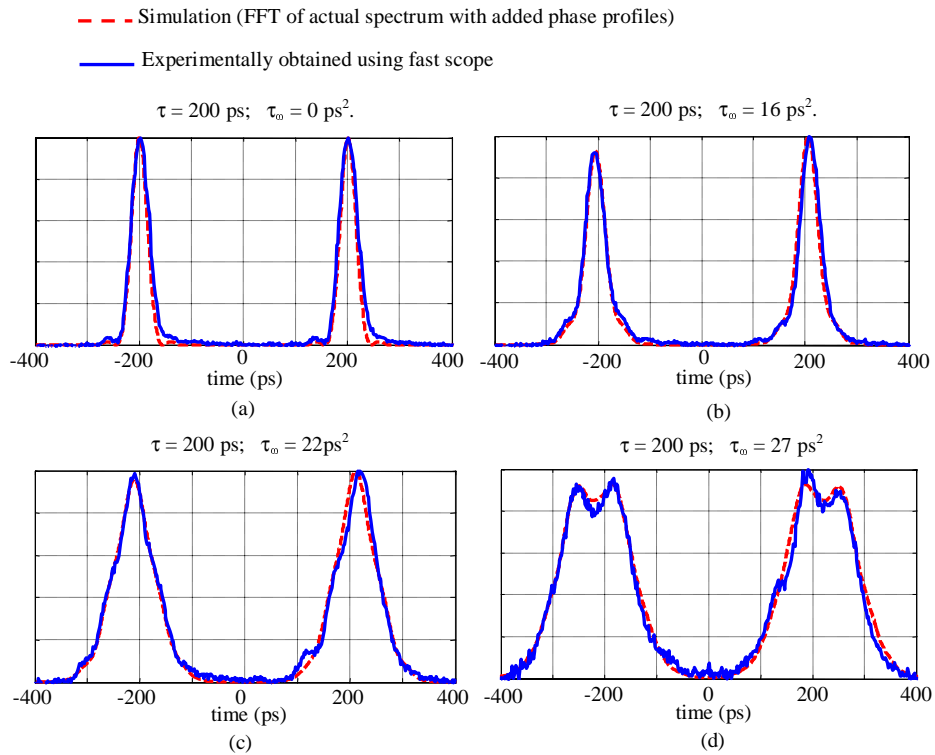


Fig. 5. Pulse experiencing constant DGD of $2\tau=400\text{ps}$ and linear DGD with $2\tau_0$ equal to (a) 0ps^2 , (b) 36ps^2 , (c) 44ps^2 , and (d) 54ps^2 .

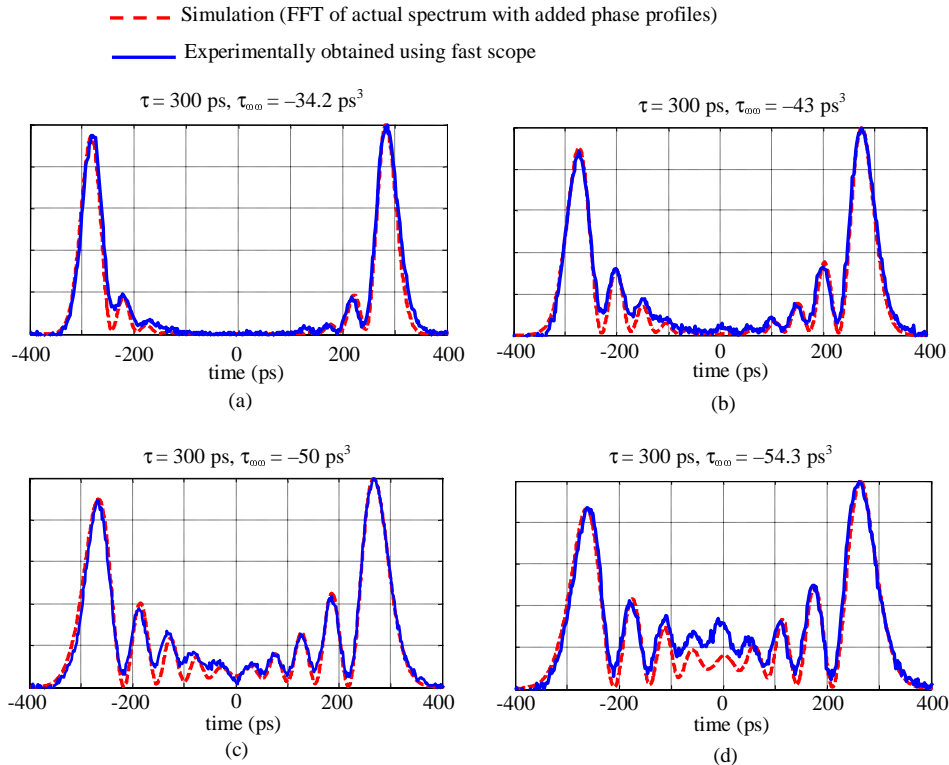


Fig. 6. Pulse experiencing constant DGD of $2\tau=600\text{ps}$ and quadratic DGD with τ_{ooo} equal to (a) -34.2ps^3 , (b) -43ps^3 , (c) -50ps^3 , and (d) -54.3ps^3 .

It is important to point out that our results are quite distinct from what would be obtained by any combination of frequency-independent DGD and isotropic frequency-dependent chromatic dispersion. This is especially clear from the data of Fig. 6. If one were to apply frequency-independent DGD and isotropic cubic spectral phase, one would indeed obtain a separated pair of pulses, both of which would have an oscillatory tail characteristic of cubic spectral phase. However, the temporal sense of the tails would be the same for both pulses – unlike the data of Fig. 6, where the oscillatory tails are time-reversed with respect to each other. The polarization-dependent chromatic dispersion produced in our apparatus is equal and opposite for the two principal states of polarization, exactly as expected for a pure DGD emulator.

Note also that the isotropic chromatic dispersion is set to zero in all of our experiments. If desired, our apparatus can be programmed for a superposition of frequency-dependent DGD and isotropic chromatic dispersion, by programming a phase equal to the superposition of a differential phase (corresponding to the desired frequency-dependent DGD) with a common-mode phase (corresponding to the desired frequency-dependent isotropic chromatic dispersion). In this case, waveforms generated for input light along either principal state of polarization would be distinct (beyond the time-reversal of Fig. 6).

The effects of the DGD emulator were also observed in the frequency domain by looking at the output spectral state-of-polarization (SOP). The frequency-dependent SOP was measured using a high resolution scanning spectral polarimeter composed of a polarization component selector and an optical spectrum analyzer running with 0.01nm 3dB spectral resolution. The polarization component selector is made up of a pair of ferroelectric liquid crystal quarter-wave retarders with fast switching optic axes, and a fixed polarizer. This setup allows four different polarization components of the input light to be measured and analyzed

at each wavelength. The reader is directed to Ref. [17] for detailed description of this spectral polarimeter design. When frequency-independent DGD is applied to the emulator to mimic a polarization maintaining fiber, the output spectral SOP traces out a circle on the Poincaré Sphere, with the circle centered about the PSP axes. As expected [2], the distance between SOP samples corresponding to adjacent optical frequency samples is constant (assuming constant frequency spacing between adjacent samples, as in our measurements). Figure 7(a) shows the spectral SOP plot of 15GHz bandwidth of the input light with zero DGD, which is a single point on the Poincaré Sphere since the light is completely polarized in one direction. Fig. 7(b) shows the spectral SOP when 60ps of frequency-independent DGD is applied to the input light, causing the light to spread out along a circular trajectory as expected.

The spectral polarization control may remind readers of a polarization pulse shaper [16, 18]. Indeed, the physical layout of the DGD emulator is similar to a polarization pulse shaper. However, the phase profiles programmed onto the SLMs are different. The polarization pulse shaper controls the phase between the two SLM layers and the polarization at each frequency sample [16]. In contrast, the DGD emulator is only interested in the differential phase between the two SLM layers; the spectral polarization change is merely an after-effect of the applied DGD. Also, because the PSP are fixed in our current apparatus, the DGD emulator does not allow arbitrary control of the spectral polarization profile, which requires the SLM to have at least two different sets of PSP — see for examples [9, 18, 19].

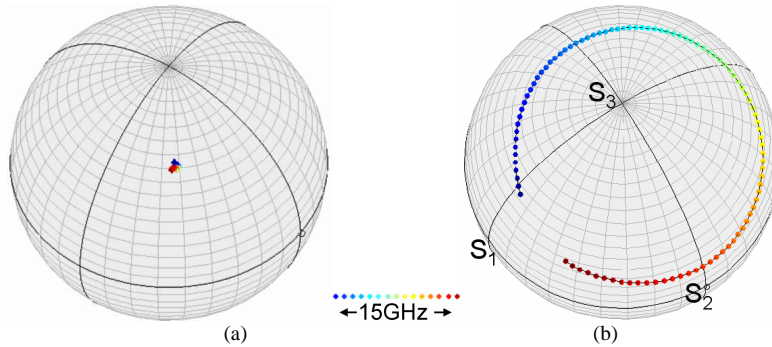


Fig. 7. Spectral SOP plot of 15GHz bandwidth at the output of the DGD emulator with constant DGD values of (a) 0, and (b) $2\tau=60$ ps. Note: the PSP (center of the circles) of the DGD emulator is polarization shifted away from 45° by the single mode fiber at the output.

To compare DGD settings with actual DGD produced, $\Delta\tau$ can be calculated from measured SOP string length l between neighboring SOP points using the equation [20]:

$$l(\omega) = (\Delta\tau(\omega) \Delta\omega) \sin(\xi) \quad (8)$$

where ξ is the angle between the input PSP and launch SOP. We worked with a simplified case when $\xi = 90^\circ$, physically meaning that the power is equally split between the slow and the fast PSP axes, and is accomplished by setting equal the heights of the time domain pulses as seen in the time domain analysis. The following table shows the DGD values which was tested up to 100ps. $\Delta\omega = 7.9 \times 10^8$ rad/s was calculated from the 1pm wavelength step of the optical spectrum analyzer at center wavelength of 1545.48nm. As can be seen from Table 1, the produced constant $\Delta\tau$ is within ± 1 ps of the specified values which the emulator was set to. This accuracy agrees with the results from the earlier time domain analysis.

Table 1. Values of measured DGD compared to the set DGD of the emulator using the frequency domain analysis.

$\Delta\tau$ setting (ps)	l (rad)	Measured $\Delta\tau$ (ps)
10	0.0078	9.87
20	0.0153	19.4
30	0.0234	29.7
40	0.0309	39.1
50	0.0394	49.9
75	0.0593	75.1
100	0.0784	99.3

Linear and quadratic DGD profiles were also tested. For linear DGD, the phase difference $2\phi(\omega)$ between the two PSP is quadratic in frequency according to Eq. (7), causing the phase change per pixel spacing $\Delta\phi(\omega)$ (and thus $l(\omega)$) to vary linearly with frequency, intersecting 0 at ω_0 . Because the PSP orientation remains fixed in our emulator, the resultant SOP vs. frequency trajectory first revolves in one direction around the Poincaré sphere and then retraces its path revolving in the opposite direction. This effect is clearly observed in the experimental results of Fig. 8(a). Since $l(\omega)$ from Eq. (8) is proportional to $\Delta\tau(\omega)$, $l(\omega)$ is also linear in frequency as shown in the measured values in Fig. 8(d). For quadratic DGD, spectral SOP looks similar to constant DGD [see Fig. 8(b)], except SOP spacing $l(\omega)$ varies quadratically with frequency, touching 0 at ω_0 as shown in Fig. 8(e). And finally, we programmed combinations of different orders of DGD. Figure 8(c) shows a sample spectral SOP with $\tau = 10\text{ps}$ and $\tau_{\omega\omega} = 34.2\text{ps}^3$ programmed into the emulator. The resultant SOP is a stretched out version of what was seen in Fig. 8(b), and the quadratic curve of $l(\omega)$ is shifted upwards by a constant of 0.0155rad due to the added constant DGD as shown in Fig. 8(f). These experimental results showed excellent agreements with our expectation, further validating the functionality of the DGD emulator.

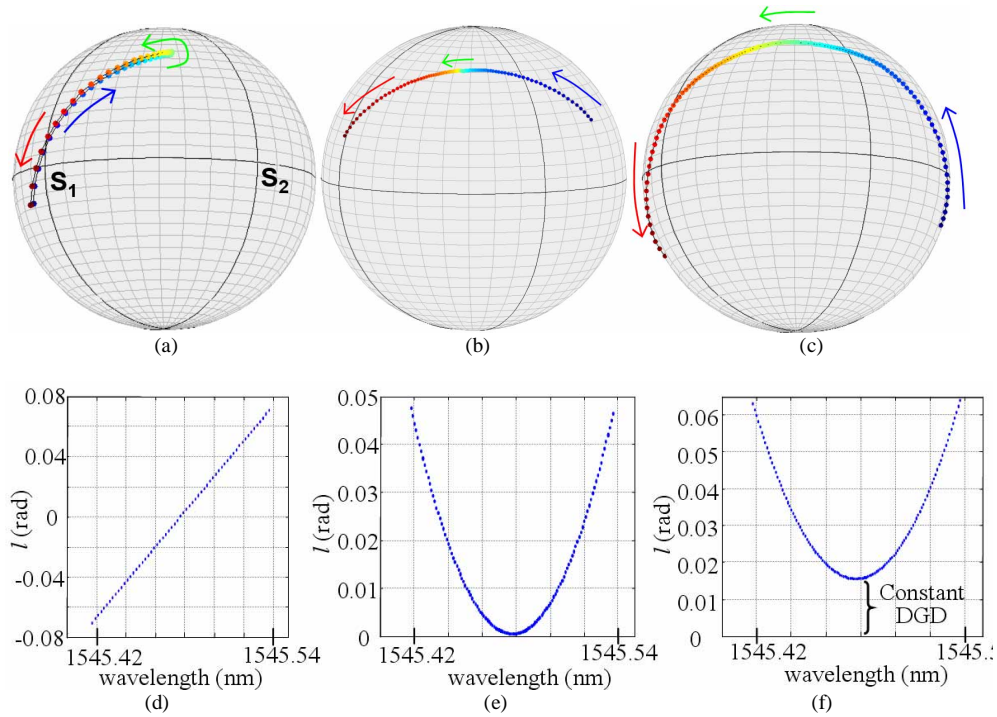


Fig. 8. Spectral SOP with (a) linear DGD of $\tau_0=11\text{ps}^2$, (b) quadratic DGD of $\tau_{000} = 34.2\text{ps}^3$, (c) combined DGD with $\tau = 10\text{ps}$ and $\tau_{000} = 34.2\text{ps}^3$. Distance between neighboring SOP points of (d) $\tau_0=11\text{ps}^2$, (e) $\tau_{000} = 34.2\text{ps}^3$, and (f) $\tau = 10\text{ps}$ and $\tau_{000} = 34.2\text{ps}^3$.

5. Conclusion and discussion

We have described a DGD emulator capable of producing complex and essentially arbitrary user-defined DGD vs. frequency profiles. This potentially powerful feature has not been demonstrated in previous PMD/DGD emulator designs. We have performed emulations of DGD profiles with constant, linear, and quadratic frequency dependences, and experimental measurements of waveforms generated by the DGD emulator agreed very well with expectation. With the capability of arbitrary DGD generation, this emulator could be programmed with algorithms to run user specified DGD evolution for systems testing of PMD tolerance and to characterize outage probability. Since DGD is produced controllably and with the capability for complex frequency dependences, techniques such as importance sampling could also be implemented by programming the emulator with user defined DGD statistics, including appropriate higher-order DGD variations. However, due to the fixed optical axis directions of the liquid crystal arrays in the SLM, the emulator does not fully mimic PMD in a long-haul optical fiber, i.e. the magnitude of the PMD vector can be varied but not its direction. In order to control the direction of the PMD vector (or PSP) in a wavelength dependent fashion, one could use a wavelength-parallel polarization controller [9] to control the PSP of each wavelength to a user specified location on the Poincaré sphere. This would give user the complete control over both the magnitude and the direction of the PMD vector $\mathbf{\Omega}(\omega)$.

We gratefully acknowledge many helpful discussions with Peter Miller of CRI Inc., Zhi Jiang for his pulse shaper setup which was used as the 20GHz bandpass filter, and the donation of the VIPA from Chris Lin of Avanex Corporation. This work was supported under NSF grant number 0501366-ECS.